

Efficient organic terahertz generator with extremely broad terahertz molecular vibrational mode-free range

Cite as: APL Mater. 11, 011101 (2023); doi: 10.1063/5.0116905

Submitted: 17 August 2022 • Accepted: 15 December 2022 •

Published Online: 3 January 2023






View Online



Export Citation



CrossMark

Bong-Rim Shin,¹  In Cheol Yu,² Myeong-Hoon Shin,¹  Mojca Jazbinsek,³  Fabian Rotermund,^{2,a)}  and O-Pil Kwon^{1,a)} 

AFFILIATIONS

¹Department of Molecular Science and Technology, Ajou University, Suwon 16499, Korea

²Department of Physics, Korea Advanced Institute of Science and Technology (KAIST), Daejeon 34141, Korea

³Institute of Computational Physics, Zurich University of Applied Sciences (ZHAW), 8401 Winterthur, Switzerland

^{a)}Authors to whom correspondence should be addressed: rotermund@kaist.ac.kr and opilkwon@ajou.ac.kr

ABSTRACT

For nonlinear optical materials to be applicable as efficient broadband terahertz (THz) wave generators, low absorption with wide transparency in the THz frequency range is highly important. In this study, we report efficient organic THz wave generators, 2-(4-hydroxystyryl)-1-methylquinolinium 4-bromobenzenesulfonate (OHQ-BBS) single crystals. Interestingly, the OHQ-BBS crystals exhibit a wide molecular vibrational mode-free range in the THz frequency region from 1.7 to 5.1 THz with an absorption coefficient of $<20 \text{ mm}^{-1}$. By optical rectification employing 130 fs pump pulses at 1300 nm wavelength, the OHQ-BBS crystals generate extremely broad, dipole-free THz waves in the range of 1.2–5.5 THz. Additionally, a THz electric field that is 20 times higher than the field generated from the widely used ZnTe inorganic crystal is achieved. Therefore, the OHQ-BBS single crystals are highly promising materials for diverse THz photonic applications.

© 2023 Author(s). All article content, except where otherwise noted, is licensed under a Creative Commons Attribution (CC BY) license (<http://creativecommons.org/licenses/by/4.0/>). <https://doi.org/10.1063/5.0116905>

I. INTRODUCTION

The research area of terahertz (THz) photonics, which is based on electromagnetic waves with a frequency in the range of 0.1–20 THz, is rapidly expanding to diverse spectroscopic and nonlinear optical applications.^{1–3} The polarization response of materials in the THz frequency range is different than in the conventional optical and radio frequency ranges.^{1,4} In the optical range with frequencies above the THz range, ultraviolet light and visible light resonate with electronic states of matter, while infrared (IR) light resonates with non-collective chemical-bond vibrations in matter. Radio waves with frequencies below the THz frequency range may excite lower frequency acoustic lattice vibrations. In contrast, the THz waves resonate with collective vibrations such as optical lattice vibrations and molecular phonon vibrations of matter.^{1,5–8} The collective phonon vibrations of (inorganic and organic) matter exist at all operating temperatures, and their absorption amplitude

cannot be ignored in a wide range of THz frequencies also for THz device materials. Therefore, the absorption characteristics that originate from the collective optical phonon vibrations of matter are critical parameters in materials for developing THz passive or active devices.

For active THz devices such as THz wave generators and detectors, it is difficult to achieve low THz absorption that would be highly beneficial for reducing the self-absorption of THz waves. Both a low-absorption coefficient α_{THz} and a wide low-absorption band (i.e., the so-called wide phonon-free range) are required. Most inorganic and organic THz device materials exhibit high absorption coefficients associated with phonon resonances over a wide THz frequency range.^{3–17} For example, an inorganic LiNbO₃ nonlinear optical crystal that has been widely used as an intense THz generator, generating up to a few MV/cm THz electric field strengths,¹⁸ exhibits many transverse optical (TO) phonon vibrations in the high THz frequency region, e.g., 4.7, 5.4, and 7.1 THz in E(TO) modes

and 7.6 and 8.2 THz in $A_1(\text{TO})$ modes.^{9–11} The absorption coefficient of LiNbO_3 rapidly increases with increasing THz frequency.¹² Moreover, the absorption coefficient of (pure and Mg-doped) congruent and stoichiometric LiNbO_3 crystals is over 20 mm^{-1} already below 3.0–3.8 THz at 300 K.¹² Consequently, the bandwidth of the generated THz waves in a LiNbO_3 crystal in a tilted-pulse-front geometry is very limited (below 3 THz).² This relation between phonon vibrations and bandwidth limitation is also observed in inorganic semiconducting crystals (e.g., ZnTe and GaP), which are widely used in THz wave generation (e.g., optical rectification) and detection [e.g., electro-optic sampling (EOS)].^{2,13–15} Note that in applications such as THz nonlinear optics including high-harmonic generation, a wide phonon-free range of THz-device materials is important.^{19–22}

In this work, we report efficient organic crystalline THz generators exhibiting a broad molecular vibrational mode-free range in a broad THz frequency range from 1.7 to 5.1 THz with an absorption coefficient of $<20 \text{ mm}^{-1}$. The organic crystals pumped by 130 fs optical pulses show very broad THz wave generation with a wide,

dimple-free spectral range from 1.2 to 5.5 THz. The dimples are defined here as the relatively sharp valley with minima-amplitude in the generated THz spectrum resulting from the self-absorption of THz waves by (molecular phonon) vibrational modes. In addition, the THz wave generation efficiency is at the top-level, similar to other benchmark organic generators (i.e., one order of magnitude higher generated THz fields compared to common inorganic generators). Therefore, the investigated organic single crystals with a broad THz molecular vibrational mode-free range, which show efficient and broadband THz generation, are highly promising for diverse THz photonic applications.

II. RESULTS AND DISCUSSION

A. Selection of THz generation materials

Recently, various organic salt crystals based on highly nonlinear optical 2-(4-hydroxystyryl)-1-methylquinolinium (OHQ) cations [Fig. 1(a)] have been developed.^{23–28} Many OHQ-based crystals

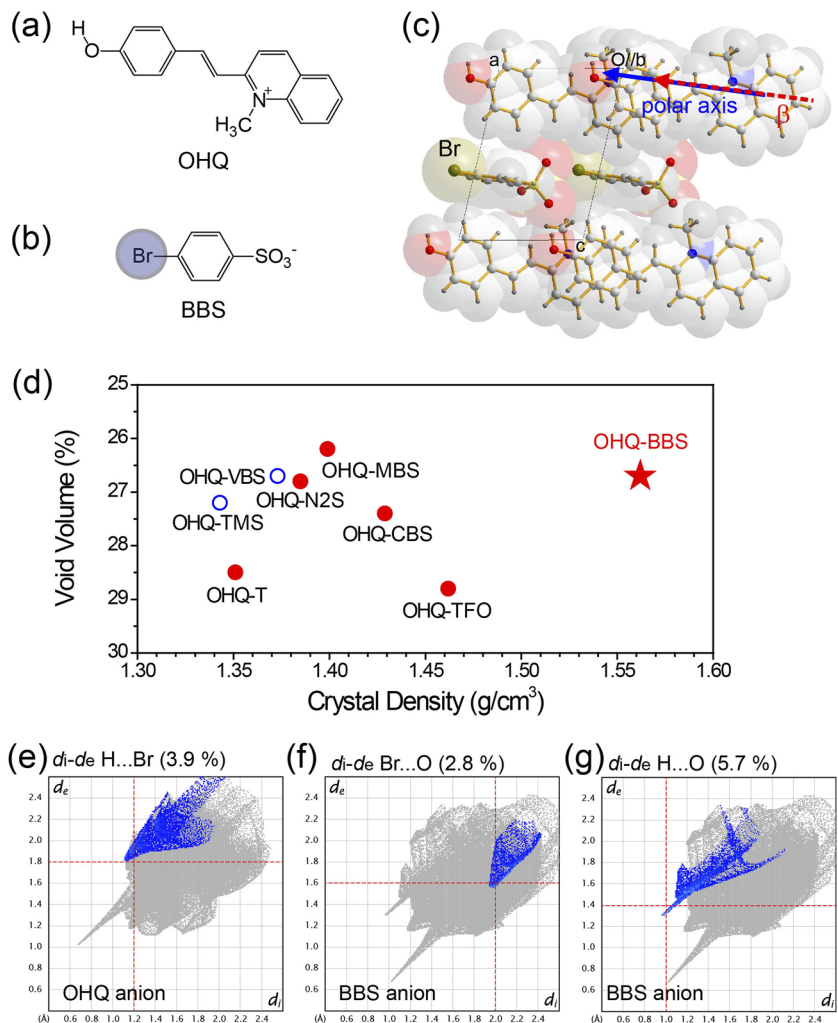


FIG. 1. (a) and (b) Chemical and (c) crystal structures of the OHQ-BBS crystals. (d) Void volume and crystal density of the OHQ-based crystals. The red closed symbols (circles and star) present the OHQ-based crystals having a close-to maximum value of the diagonal order parameter of ~ 1.0 , whereas the blue open symbols present crystals with a relatively low diagonal order parameter. Intermolecular interactions in the OHQ-BBS crystals presenting representative Hirshfeld surfaces of (e) OHQ cation and (f) and (g) BBS anion.

exhibit top-level macroscopic optical nonlinearity and the possibility for bulk crystal growth. With varying molecular counteranions [see, e.g., Fig. 1(b)], the OHQ-based crystals have shown remarkable changes in their material parameters, such as physical and optical properties, as well as crystal characteristics, such as crystal structure, morphology, and the direction of the polar axis, which are important for nonlinear optical applications.^{23–28} As each of the OHQ-based crystals is optimally selected for specific target nonlinear optical applications, a limitation in THz device materials (e.g., THz absorption and generation in this study) can be overcome. Among the various OHQ-based crystals, we chose 2-(4-hydroxystyryl)-1-methylquinolinium 4-bromobenzenesulfonate (OHQ-BBS) for the reasons discussed below.

For the optimal selection for THz wave generation, we considered various material parameters and crystal characteristics of the OHQ-based crystals. The optical-to-THz (power) conversion efficiency during optical rectification is proportional to the square of the effective macroscopic second-order nonlinear optical coefficient

of the THz generation crystals.^{16,29} The macroscopic optical nonlinearity in organic crystals increases with an increase in the so-called diagonal order parameter $\cos^3 \theta_p$, where θ_p is the angle between the polar axis of the crystal and the main charge-transfer axis (i.e., the main direction of the first hyperpolarizability) of the cationic chromophores.¹⁶ The order parameter $\cos^3 \theta_p$ reaches the maximum value when the chromophores (OHQ cations in this study) are aligned perfectly parallel, as shown in an example of the OHQ-based OHQ-BBS crystals in Fig. 1(c).²⁶ The crystal structure of the OHQ-BBS crystals is obtained from Ref. 26. Figure 1(d) shows the important crystal characteristics (void volume and crystal density) for THz wave absorption and generation for the previously reported OHQ-based crystals possessing an acentric crystal space group and, therefore, a non-zero order parameter.^{23–28} Since the OHQ-based crystals possess a wide range of order parameter $\cos^3 \theta_p$,^{23–28} in Fig. 1(d), they are classified into two groups, shown as open and closed symbols. The order parameter $\cos^3 \theta_p$ is obtained and evaluated from Refs. 23–28. The OHQ-based crystals presented with red

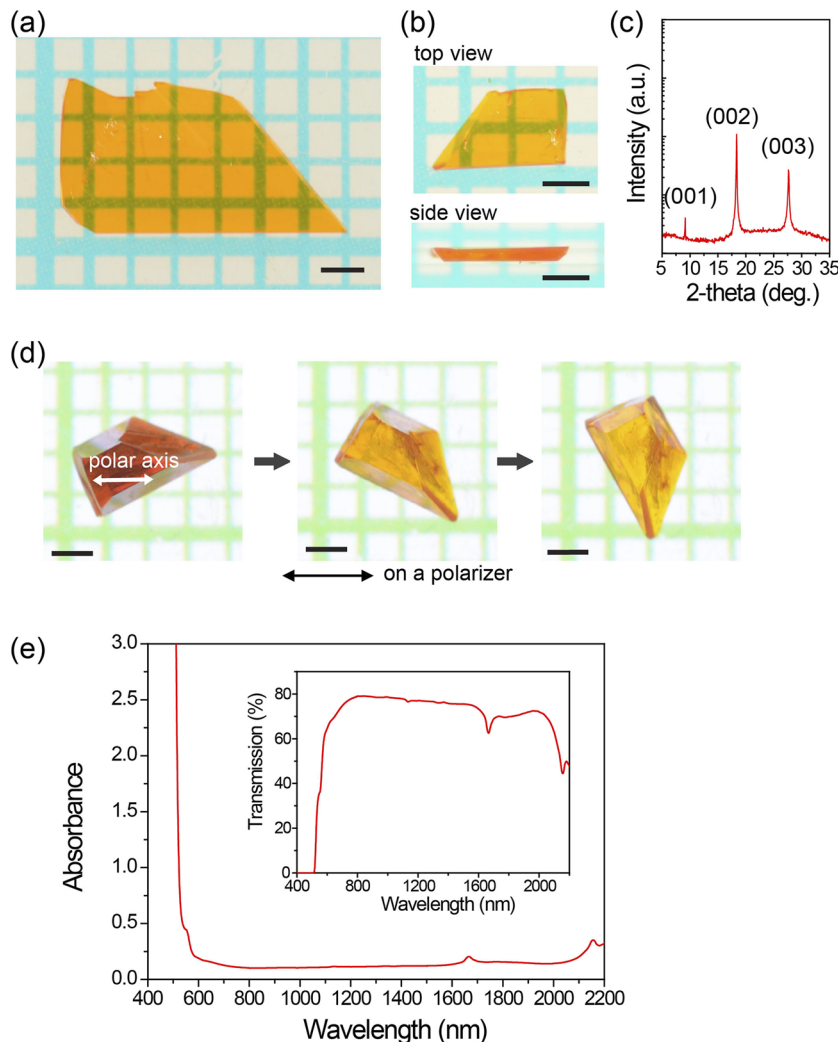


FIG. 2. (a) and (b) Photographs of the as-grown OHQ-BBS single crystals (scale bar: 1 mm). (c) X-ray diffraction reflection pattern of the OHQ-BBS single crystal. (d) Photographs taken on a polarizer with a rotation of the OHQ-BBS crystal (scale bar: 1 mm). The black and white double arrows are the direction of the polarization of the light and the polar axis of the OHQ-BBS crystals, respectively. (e) Transmittance of a 0.1 mm thick OHQ-BBS crystal measured using unpolarized light.

closed symbols (circles and star) show a close-to maximum value of the diagonal order parameter of $\cos^3 \theta_p \approx 1.0$ for the OHQ-BBS, OHQ-CBS (CBS = 4-chlorobenzenesulfonate), OHQ-MBS (MBS = 4-methoxybenzenesulfonate), OHQ-N2S (N2S = naphthalene-2-sulfonate), and OHQ-T (T = 4-methylbenzenesulfonate) crystals, as well as $\cos^3 \theta_p = 0.94$ for the OHQ-TFO (TFO = 4-(trifluoromethoxy)benzenesulfonate) crystals. In contrast, the OHQ-based crystals presented with blue open circles show a relatively low diagonal order parameter, 0.6 and 0.01 for the OHQ-VBS (VBS = 4-vinylbenzenesulfonate) and OHQ-TMS (TMS = 2,4,6-trimethylbenzenesulfonate) crystals, respectively.^{23–28} Consequently, in terms of macroscopic optical nonlinearity, the OHQ-based crystals denoted by red closed symbols in Fig. 1(d) are better candidates for THz applications than those with blue open symbols.

The absorption coefficient of organic crystals in the THz frequency range often decreases with stronger intermolecular interactions, higher crystal density, higher melting temperature, and lower void volume.^{7,8} Figure 1(d) shows the void volume and the crystal density of the OHQ-based crystals. The crystal density was obtained from the corresponding crystal structure, and the void volume was calculated using the program Mercury 4.3.0, Cambridge Crystallographic Data Centre (CCDC).³⁰ The void volumes for OHQ-T, OHQ-CBS, OHQ-N2S, and OHQ-TFO were obtained from Ref. 7, and for OHQ-MBS, OHQ-VBS, and OHQ-TMS, they were newly calculated in this study. Among the various OHQ-based crystals, the OHQ-BBS crystals possess the highest crystal density [Fig. 1(d)]. In addition, the void volume of the OHQ-BBS crystals is relatively small [Fig. 1(d)]. Moreover, the OHQ-BBS crystals exhibit the highest melting temperature of 321 °C.²⁶ The OHQ-T, OHQ-MBS, OHQ-N2S, and OHQ-CBS crystals exhibit lower melting temperatures of 285, 286, 293, and 302 °C, respectively.^{23,25,26,28} The reason for the low void volume, high crystal density, and high melting temperature of the OHQ-BBS crystals may be attributed to the additional intermolecular interactions created by the heavy-atom brominated substituent on the 4-bromobenzenesulfonate (BBS) anion.³¹ The representative intermolecular interactions involving Br are shown in Figs. 1(e) and 1(f) with Hirshfeld surfaces.^{32–34} In addition, in the OHQ-BBS crystals, the strong intermolecular interactions appearing in other OHQ-based crystals were maintained; an example is shown in Fig. 1(g). Consequently, the OHQ-BBS crystals with a large macroscopic optical nonlinearity, low void volume, high crystal density, and high melting temperature may exhibit interesting THz absorption and generation characteristics.

B. As-grown OHQ-BBS single crystals suitable for THz photonics

The bulk OHQ-BBS single crystals were grown using the slow cooling method in methanol and acetonitrile mixed solvent. Figures 2(a), 2(b), and 2(d) show the photographs of the as-grown OHQ-BBS single crystals. The OHQ-BBS single crystals exhibit good crystal morphology with a plate shape having two parallel surfaces and regular thickness [top and side views in Fig. 2(b)]. The morphology of the OHQ-BBS single crystals with a plate shape is beneficial for most optical experiments, including THz wave generation. In addition, the area of the largest surface in the as-grown OHQ-BBS crystals is greater than 15 mm² [Fig. 2(a)].

In THz wave generation crystals, the direction of the polar axis of the crystals, crystallographic facet, and transparency of the

optical pump wavelength are important. To achieve the maximum conversion efficiency in a collinear THz generation geometry at a normal incident optical pump, the optimal direction of the polar axis is the in-plane polar axis; that is, the polar axis is parallel to the largest surface of the organic THz crystals.^{16,28} The largest plane of the as-grown OHQ-BBS crystals is the crystallographic (001) plane, which was determined by x-ray diffraction experiments [Fig. 2(c)]. Figure 2(d) shows the photographs of an OHQ-BBS crystal with a rotation on a polarizer that determines the direction of the polar axis of the OHQ-BBS crystals. When the OHQ-BBS crystals appear darkest in transmission during the rotation [left photograph in Fig. 2(d)], the polarization direction of the light (black double arrow) is parallel to the direction of the polar axis (white double arrow) in the OHQ-BBS crystals. As shown in Fig. 1(c), the direction of the polar axis in the OHQ-BBS crystals is completely parallel to the direction of the first hyperpolarizability β of the OHQ cation. Note that the direction of the first hyperpolarizability β of the OHQ cation in the OHQ-BBS crystals is assumed to be identical to that in the isomorphous OHQ-CBS crystals.²⁶ In the OHQ-BBS single crystals, the direction of the polar axis is almost parallel to the (001) crystal facet with a very small angle of $\sim 8^\circ$. The practically in-plane polar axis allows for the full projection of the polar axis in a simple THz generation geometry and, therefore, leads to the maximum effective macroscopic optical nonlinearity.

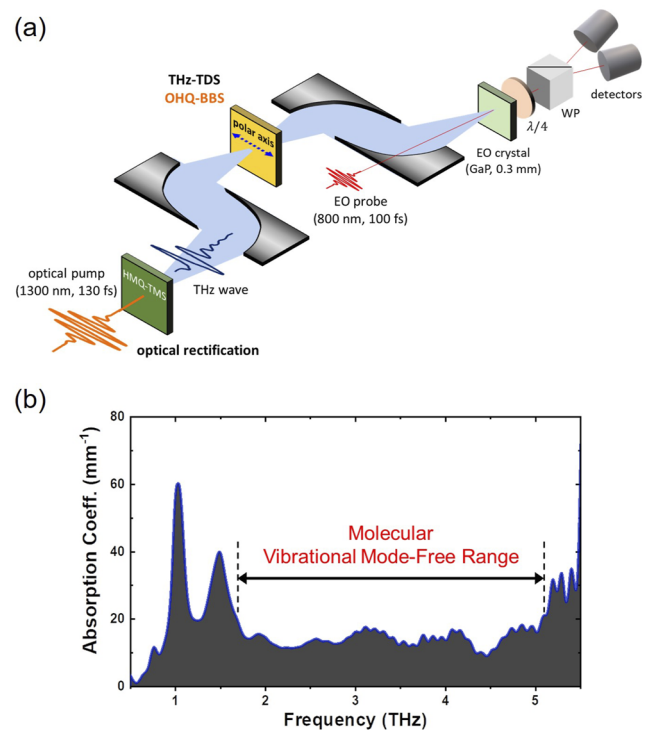


FIG. 3. (a) Schematic diagram of the THz-TDS setup for the absorption coefficient measurement of the OHQ-BBS crystals and (b) absorption coefficient, α_{THz} , of the OHQ-BBS crystals along the polar axis in the THz frequency range. The molecular vibrational mode-free range is very broad, 1.7–5.1 THz at $\alpha_{\text{THz}} < 20 \text{ mm}^{-1}$.

Figure 2(e) shows the transmittance curve of a 0.1 mm thick OHQ-BBS crystal measured using unpolarized light. The OHQ-BBS crystal exhibits a wide transparency range. The cutoff wavelength of absorption is at ~ 530 nm, and a very good transparency is maintained at up to 1630 nm. Therefore, for THz wave generation, the OHQ-BBS crystals can be pumped at widely used optical wavelengths in near-IR and IR regions. In this study, the OHQ-BBS crystals are pumped at a wavelength of 1300 nm for the demonstration of efficient THz wave generation.

C. Wide THz molecular vibrational mode-free range of OHQ-BBS single crystals

The OHQ-BBS single crystals exhibit a unique absorption behavior, specifically a very broad molecular vibrational mode-free range in the THz frequency range. The absorption coefficient α_{THz} of the OHQ-BBS crystals along the polar axis is measured by THz time-domain spectroscopy (THz TDS), as schematically shown in Fig. 3(a). A well-known organic HMQ-TMS (HMQ = 2-(4-hydroxy-3-methoxystyryl)-1-methylquinolinium) crystal³⁵ is used as the THz generator. The generated THz waves propagating both in the air and through the OHQ-BBS crystal are detected via EOS using a 0.3 mm-thick GaP with 100 fs probe pulses at a wavelength of 800 nm. Subsequently, the refractive index is obtained from these THz TDS results and the absorption coefficient of the crystal is calculated by

the thin-film transmittance approximation method,^{36,37} where the Fresnel loss at the interface and the multiple reflection in the sample are taken into account.

Figure 3(b) shows the absorption coefficient α_{THz} of the OHQ-BBS crystals along the polar axis in the THz frequency range. The OHQ-BBS crystals exhibit a very broad THz molecular vibrational mode-free range of 1.7–5.1 THz that is here defined for low absorption coefficients $\alpha_{\text{THz}} < 20 \text{ mm}^{-1}$. This broad THz molecular vibrational mode-free range provides many advantages for THz photonic applications. Note that many benchmark organic THz salt crystals along the polar axis exhibit many strong absorption peaks in the 1.7–5.1 THz range, e.g., 2.0, 3.1, and 3.8 THz for HMQ-T crystals, 2.2, 2.9, 3.2, and 3.9 THz for HM6FQ-T, 2.3 and 3.7 THz for OHQ-TFO crystals, and 1.8, 3.6, and 4.1 THz for HMB-TMS (HMB = 2-(4-hydroxy-3-methoxystyryl)-3-methylbenzothiazol-3-ium) crystals.^{16,27,38–42} In addition, non-ionic benchmark organic THz crystals also exhibit strong absorption peaks in this range, e.g., 2.9 and 4.5 THz for non-ionic OH1 crystals.^{43,44}

In THz wave generation, the OHQ-BBS crystals may result in low self-absorption of the generated THz waves, leading to a high conversion efficiency. In addition, no absorption peak (i.e., no strong molecular phonon vibrations) in the 1.7–5.1 THz range may result in a wide generated spectrum without dimples and strong modulations as discussed in Sec. II D. In THz nonlinear optics, such as frequency

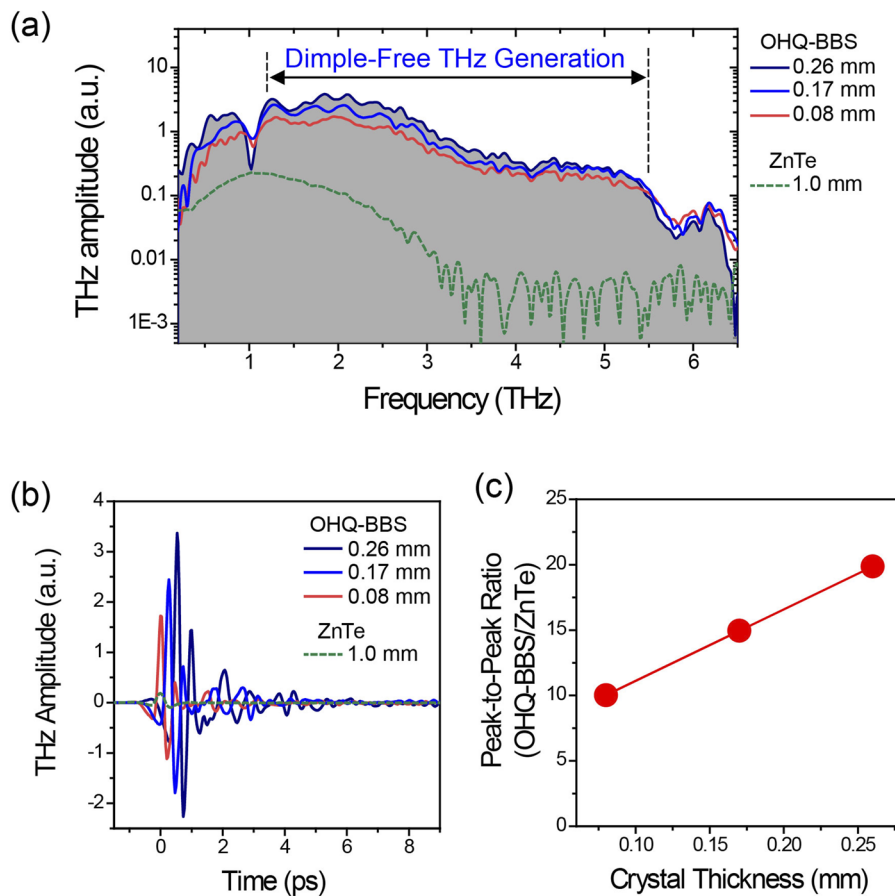


FIG. 4. THz wave spectra generated in the OHQ-BBS crystals with different crystal thicknesses of 0.08, 0.17, and 0.26 mm and a ZnTe crystal with a thickness of 1.0 mm. (a) Frequency spectra and (b) time traces. (c) The corresponding peak-to-peak ratio of the THz amplitude of the OHQ-BBS crystals relative to the ZnTe crystal (in time domain).

conversion and cross-phase modulation, the OHQ-BBS crystals can allow a wide-targeted THz frequency range with a very small loss of amplitude of the THz pump.

D. Broadband THz generation of OHQ-BBS single crystals

The results of THz wave generation with the OHQ-BBS crystals are shown in Fig. 4. For the experiments, a similar setup shown in Fig. 3(a) for THz wave generation in the HMQ-TMS crystal is used. The OHQ-BBS crystals are pumped at the wavelength of 1300 nm with 130 fs long pulses at a repetition rate of 1 kHz. The THz waves generated by optical rectification in these crystals with different thicknesses of 0.08, 0.17, and 0.26 mm are detected via conventional EOS at 800 nm with 100 fs probe pulses.

Figure 4(a) shows the THz spectra generated by the OHQ-BBS crystals. The wide molecular vibrational mode-free range of 1.7–5.1 THz of the OHQ-BBS crystals results in broad, dimple-free THz wave generation. The generated THz waves show an extremely broad spectrum, except for the absorption-induced dimple at around 1 THz. Furthermore, the OHQ-BBS crystals exhibit a high optical-to-THz conversion efficiency beyond the broad dimple-free THz generation frequency of 1.2–5.5 THz.

The THz fields generated from the OHQ-BBS crystals are compared with those of the ZnTe crystal, as shown in Figs. 4(b) and 4(c). The OHQ-BBS crystals show a much higher optical-to-THz conversion efficiency than the reference crystal, which increases linearly with the crystal thickness. The linear increase in the generated THz field with the thickness indicates a very good phase matching with the optical-to-THz conversion efficiency not limited by the coherence length yet in this thickness range. Consequently, the THz generation performance can be further improved by optimizing the sample thickness.

Although the thickness of the OHQ-BBS crystal was still not fully optimized, this crystal with a thickness of 0.26 mm provides ~20 times the optical-to-THz conversion efficiency as does the 1.0 mm-thick ZnTe crystal at the pump wavelength of 1300 nm [Fig. 4(c)] and the performance of THz wave generation is already comparable to that of benchmark organic crystals. For example, when pumped at 1300 nm, the optical-to-THz conversion efficiency is more than 24 times higher for the 0.39 mm-thick HMQ-T crystals, 25 times for the 0.38 mm-thick HM6FQ-T crystals, and ~16 times for the 0.52 mm-thick OHQ-TFO crystals^{38,39} than that achieved in the 1.0 mm-thick ZnTe crystals. In addition, note that the optical-to-THz conversion efficiency of many benchmark organic THz crystals is typically about ten times higher than that reported for a 0.3 mm-thick GaP crystal, when pumped at infrared wavelengths (1250–1500 nm).^{45,46} Consequently, the OHQ-BBS crystals are beneficial for efficient THz wave generation with a high conversion efficiency and generate dimple-free broad THz waves in the frequency range of 1.2–5.5 THz.

III. CONCLUSION

In summary, we reported an efficient broadband THz generator OHQ-BBS with a wide molecular vibrational mode-free range in the THz frequency range of 1.7–5.1 THz. The as-grown OHQ-BBS crystals generated extremely broad, dimple-free THz waves in the range of 1.2–5.5 THz that could not be fully covered by the standard ZnTe and other existing inorganic THz generators. Therefore,

the as-grown OHQ-BBS crystals are promising materials for THz photonics.

ACKNOWLEDGMENTS

This work was supported by the National Research Foundation of Korea (NRF) funded by the Ministry of Science, ICT and Future Planning, Korea (Grant Nos. 2021R1A2C1005012, 2021R1A5A6002853, 2019K1A3A1A14057973, and 2019R1A2C3003504), Institute for Information and Communications Technology Planning and Evaluation (IITP) grant funded by the Korea government (MSIT) (Grant No. 2022-0-00624), and Swiss National Science Foundation (SNSF), Switzerland (Grant No. IZKSZ2_188194).

AUTHOR DECLARATIONS

Conflict of Interest

The authors have no conflicts to disclose.

Author Contributions

B. R. Shin and I. C. Yu contributed equally to this work.

Bong-Rim Shin: Formal analysis (lead); Writing – original draft (lead). **In Cheol Yu:** Formal analysis (lead); Writing – original draft (lead). **Myeong-Hoon Shin:** Formal analysis (equal). **Mojca Jazbinsek:** Formal analysis (supporting); Writing – review & editing (supporting). **Fabian Rotermund:** Formal analysis (lead); Supervision (lead); Writing – original draft (lead); Writing – review & editing (lead). **O-Pil Kwon:** Formal analysis (lead); Supervision (lead); Writing – original draft (lead); Writing – review & editing (lead).

DATA AVAILABILITY

The data that support the findings of this study are available from the corresponding authors upon reasonable request.

REFERENCES

- 1 T. Kampfrath, K. Tanaka, and K. A. Nelson, “Resonant and nonresonant control over matter and light by intense terahertz transients,” *Nat. Photonics* **7**, 680–690 (2013).
- 2 J. A. Fülöp, S. Tzortzakakis, and T. Kampfrath, “Laser-driven strong-field terahertz sources,” *Adv. Opt. Mater.* **8**, 1900681 (2019).
- 3 T. L. Cocker, V. Jelic, R. Hillenbrand, and F. A. Hegmann, “Nanoscale terahertz scanning probe microscopy,” *Nat. Photonics* **15**, 558–569 (2021).
- 4 M. Jazbinsek, U. Puc, A. Abina, and A. Zidansek, “Organic crystals for THz photonics,” *Appl. Sci.* **9**, 882 (2019).
- 5 S. Fratini, S. Ciuchi, D. Mayou, G. T. de Laissardière, and A. Troisi, “A map of high-mobility molecular semiconductors,” *Nat. Mater.* **16**, 998–1002 (2017).
- 6 G. Schweicher, G. D’Avino, M. T. Ruggiero, D. J. Harkin, K. Broch, D. Venkateshvaran, G. Liu, A. Richard, C. Ruzié, J. Armstrong, A. R. Kennedy, K. Shankland, K. Takimiya, Y. H. Geerts, J. A. Zeitler, S. Fratini, and H. Siringhaus, “Chasing the ‘killer’ phonon mode for the rational design of low-disorder, high-mobility molecular semiconductors,” *Adv. Mater.* **31**, 1902407 (2019).

- ⁷G. E. Yoon, J. H. Seok, U. Puc, B. R. Shin, W. Yoon, H. Yun, D. Kim, I. C. Yu, F. Rotermund, M. Jazbinsek, and O. P. Kwon, "Phonon-suppressing intermolecular adhesives: Catechol-based broadband organic THz generators," *Adv. Sci.* **9**, 2201391 (2022).
- ⁸J. Kim, Y. C. Park, J. H. Seok, M. Jazbinsek, and O. P. Kwon, "Solid-state molecular motions in organic THz generators," *Adv. Opt. Mater.* **9**, 2001521 (2021).
- ⁹A. Ridah, M. D. Fontana, and P. Bourson, "Temperature dependence of the Raman modes in LiNbO₃ and mechanism of the phase transition," *Phys. Rev. B* **56**, 5967 (1997).
- ¹⁰Y. Repelin, E. Husson, F. Bennani, and C. Proust, "Raman spectroscopy of lithium niobate and lithium tantalate. Force field calculations," *J. Phys. Chem. Solids* **60**, 819–825 (1999).
- ¹¹V. Caciuc, A. V. Postnikov, and G. Borstel, "Ab initio structure and zone-center phonons in LiNbO₃," *Phys. Rev. B* **61**, 8806 (2000).
- ¹²L. Pálfalvi, J. Hebling, J. Kuhl, Á. Péter, and K. Polgár, "Temperature dependence of the absorption and refraction of Mg-doped congruent and stoichiometric LiNbO₃ in the THz range," *J. Appl. Phys.* **97**, 123505 (2005).
- ¹³G. Gallot, J. Zhang, R. W. McGowan, T.-I. Jeon, and D. Grischkowsky, "Measurements of the THz absorption and dispersion of ZnTe and their relevance to the electro-optic detection of THz radiation," *Appl. Phys. Lett.* **74**, 3450 (1999).
- ¹⁴M. Schall, M. Walther, and P. U. Jepsen, "Fundamental and second-order phonon processes in CdTe and ZnTe," *Phys. Rev. B* **64**, 094301 (2001).
- ¹⁵Q. Wu and X.-C. Zhang, "7 terahertz broadband GaP electro-optic sensor," *Appl. Phys. Lett.* **70**, 1784 (1997).
- ¹⁶S. J. Kim, B. J. Kang, U. Puc, W. T. Kim, M. Jazbinsek, F. Rotermund, and O. P. Kwon, "Highly nonlinear optical organic crystals for efficient terahertz wave generation, detection, and applications," *Adv. Opt. Mater.* **9**, 2101019 (2021).
- ¹⁷P. D. Cunningham and L. M. Hayden, "Optical properties of DAST in the THz range," *Opt. Express* **18**, 23620–23625 (2010).
- ¹⁸X.-J. Wu, J.-L. Ma, B.-L. Zhang, S.-S. Chai, Z.-J. Fang, C.-Y. Xia, D.-Y. Kong, J.-G. Wang, H. Liu, C.-Q. Zhu, X. Wang, C.-J. Ruan, and Y.-T. Li, "Highly efficient generation of 0.2 mJ terahertz pulses in lithium niobate at room temperature with sub-50 fs chirped Ti:sapphire laser pulses," *Opt. Express* **26**, 7107–7116 (2018).
- ¹⁹K. Lee, J. Park, B. J. Kang, W. T. Kim, H. D. Kim, S. Baek, K. J. Ahn, B. Min, and F. Rotermund, "Electrically controllable terahertz second-harmonic generation in GaAs," *Adv. Opt. Mater.* **8**, 2000359 (2020).
- ²⁰C. Vaswani, M. Mootz, C. Sundahl, D. H. Mudiyansele, J. H. Kang, X. Yang, D. Cheng, C. Huang, R. H. J. Kim, Z. Liu, L. Luo, I. E. Perakis, C. B. Eom, and J. Wang, "Terahertz second-harmonic generation from lightwave acceleration of symmetry-breaking nonlinear supercurrents," *Phys. Rev. Lett.* **124**, 207003 (2020).
- ²¹H. A. Hafez, S. Kovalev, J.-C. Deinert, Z. Mics, B. Green, N. Awari, M. Chen, S. Gernianskiy, U. Löhnert, J. Teichert, Z. Wang, K.-J. Tielrooij, Z. Liu, Z. Chen, A. Narita, K. Müllen, M. Bonn, M. Gensch, and D. Turchinovich, "Extremely efficient terahertz high-harmonic generation in graphene by hot Dirac fermions," *Nature* **561**, 507–511 (2018).
- ²²O. Schubert, M. Hohenleutner, F. Langer, B. Urbaneck, C. Lange, U. Huttner, D. Golde, T. Meier, M. Kira, S. W. Koch, and R. Huber, "Sub-cycle control of terahertz high-harmonic generation by dynamical Bloch oscillations," *Nat. Photonics* **8**, 119–123 (2014).
- ²³S.-H. Lee, B.-J. Kang, J.-S. Kim, B.-W. Yoo, J.-H. Jeong, K.-H. Lee, M. Jazbinsek, J. W. Kim, H. Yun, J. Kim, Y. S. Lee, F. Rotermund, and O.-P. Kwon, "New acentric core structure for organic electrooptic crystals optimal for efficient optical-to-THz conversion," *Adv. Opt. Mater.* **3**, 756–762 (2015).
- ²⁴J.-S. Kim, S.-H. Lee, M. Jazbinsek, H. Yun, J. Kim, Y. S. Lee, J. W. Kim, F. Rotermund, and O.-P. Kwon, "New phenolic N-methylquinolinium single crystals for second-order nonlinear optics," *Opt. Mater.* **45**, 136–140 (2015).
- ²⁵S.-C. Lee, B. J. Kang, M.-J. Koo, S.-H. Lee, J.-H. Han, J.-Y. Choi, W. T. Kim, M. Jazbinsek, H. Yun, D. Kim, F. Rotermund, and O.-P. Kwon, "New electro-optic salt crystals for efficient terahertz wave generation by direct pumping at Ti:sapphire wavelength," *Adv. Opt. Mater.* **5**, 1600758 (2017).
- ²⁶S.-J. Lee, B. J. Kang, M.-H. Shin, S.-C. Lee, S.-H. Lee, M. Jazbinsek, H. Yun, D. Kim, F. Rotermund, and O.-P. Kwon, "Efficient optical-to-THz conversion organic crystals with simultaneous electron withdrawing and donating halogen substituents," *Adv. Opt. Mater.* **6**, 1700930 (2018).
- ²⁷M. H. Shin, W. T. Kim, S. I. Kim, S. H. Lee, I. C. Yu, M. Jazbinsek, W. Yoon, H. Yun, D. Kim, F. Rotermund, and O. P. Kwon, "Efficient gap-free broadband terahertz generators based on new organic quinolinium single crystals," *Adv. Opt. Mater.* **7**, 1900953 (2019).
- ²⁸J.-Y. Choi, S.-J. Lee, S.-C. Lee, C.-U. Jeong, M. Jazbinsek, H. Yun, B. J. Kang, F. Rotermund, and O.-P. Kwon, "Quinolinium single crystals with a high optical nonlinearity and unusual out-of-plane polar axis," *J. Mater. Chem. C* **5**, 12602 (2017).
- ²⁹J. Hebling, K.-L. Yeh, M. C. Hoffmann, B. Bartal, and K. A. Nelson, "Generation of high-power terahertz pulses by tilted-pulse-front excitation and their application possibilities," *J. Opt. Soc. Am. B* **25**, B6–B19 (2008).
- ³⁰See www.ccdc.cam.ac.uk for Mercury 4.3.0 program, Cambridge Crystallographic Data Centre (CCDC).
- ³¹A. M. S. Riel, R. K. Rowe, E. N. Ho, A.-C. C. Carlsson, A. K. Rappé, O. B. Berryman, and P. S. Ho, "Hydrogen bond enhanced halogen bonds: A synergistic interaction in chemistry and biochemistry," *Acc. Chem. Res.* **52**, 2870–2880 (2019).
- ³²M. A. Spackman and J. J. McKinnon, "Fingerprinting intermolecular interactions in molecular crystals," *CrystEngComm* **4**, 378–392 (2002).
- ³³J. J. McKinnon, D. Jayatilaka, and M. A. Spackman, "Towards quantitative analysis of intermolecular interactions with Hirshfeld surfaces," *Chem. Commun.* **2007**, 3814–3816.
- ³⁴M. A. Spackman and D. Jayatilaka, "Hirshfeld surface analysis," *CrystEngComm* **11**, 19–32 (2009).
- ³⁵J.-H. Jeong, B.-J. Kang, J.-S. Kim, M. Jazbinsek, S.-H. Lee, S.-C. Lee, I.-H. Baek, H. Yun, J. Kim, Y. S. Lee, J.-H. Lee, J.-H. Kim, F. Rotermund, and O.-P. Kwon, "High-power broadband organic THz generator," *Sci. Rep.* **3**, 3200 (2013).
- ³⁶P. U. Jepsen and B. M. Fisher, "Dynamic range in terahertz time-domain transmission and reflection spectroscopy," *Opt. Lett.* **30**, 29 (2005).
- ³⁷S. W. King and M. Milosevic, "A method to extract absorption coefficient of thin films from transmission spectra of the films on thick substrates," *J. Appl. Phys.* **111**, 073109 (2012).
- ³⁸P.-J. Kim, J.-H. Jeong, M. Jazbinsek, S.-B. Choi, I.-H. Baek, J.-T. Kim, F. Rotermund, H. Yun, Y. S. Lee, P. Günter, and O.-P. Kwon, "Highly efficient organic THz generator pumped at near-infrared: Quinolinium single crystals," *Adv. Funct. Mater.* **22**, 200 (2012).
- ³⁹S.-H. Lee, M.-J. Koo, K.-H. Lee, M. Jazbinsek, B.-J. Kang, F. Rotermund, and O.-P. Kwon, "Quinolinium-based organic electro-optic crystals: Crystal characteristics in solvent mixtures and optical properties in the terahertz range," *Mater. Chem. Phys.* **169**, 62 (2016).
- ⁴⁰S.-I. Kim, B. J. Kang, C.-U. Jeong, M.-H. Shin, W. T. Kim, M. Jazbinsek, W. Yoon, H. Yun, D. Kim, F. Rotermund, and O.-P. Kwon, "Fluorinated organic electro-optic quinolinium crystals for THz wave generation," *Adv. Opt. Mater.* **7**, 1801495 (2019).
- ⁴¹S. H. Lee, J. Lu, S. J. Lee, J. H. Han, C. U. Jeong, S. C. Lee, X. Li, M. Jazbinsek, W. Yoon, H. Yun, B. J. Kang, F. Rotermund, K. A. Nelson, and O. P. Kwon, "Benzothiazolium single crystals: A new class of nonlinear optical crystals with efficient THz wave generation," *Adv. Mater.* **29**, 1701748 (2017).
- ⁴²J. Lu, S.-H. Lee, X. Li, S.-C. Lee, J.-H. Han, O.-P. Kwon, and K. A. Nelson, "Efficient terahertz generation in highly nonlinear organic crystal HMB-TMS," *Opt. Express* **26**, 030786 (2018).
- ⁴³O.-P. Kwon, S.-J. Kwon, M. Jazbinsek, F. D. J. Brunner, J.-I. Seo, C. Hunziker, A. Schneider, H. Yun, Y.-S. Lee, and P. Günter, "Organic phenolic configurationally locked polyene single crystals for electro-optic and terahertz wave applications," *Adv. Funct. Mater.* **18**, 3242 (2008).
- ⁴⁴A. Majkić, M. Zgonik, A. Petelin, M. Jazbinsek, B. Ruiz, C. Medrano, and P. Günter, "Terahertz source at 9.4 THz based on a dual-wavelength infrared laser and quasi-phase matching in organic crystals OH1," *Appl. Phys. Lett.* **105**, 141115 (2014).

⁴⁵G. A. Valdivia-Berroeta, E. W. Jackson, K. C. Kenney, A. X. Wayment, I. C. Tangen, C. B. Bahr, S. J. Smith, D. J. Michaelis, and J. A. Johnson, "Designing non-centrosymmetric molecular crystals: Optimal packing may be just one carbon away," *Adv. Funct. Mater.* **30**, 1904786 (2020).

⁴⁶G. A. Valdivia-Berroeta, I. C. Tangen, C. B. Bahr, K. C. Kenney, E. W. Jackson, J. DeLagange, D. J. Michaelis, and J. A. Johnson, "Crystal growth, terahertz generation, and optical characterization of EHPSI-4NBS," *J. Phys. Chem. C* **125**, 16097 (2021).